Materials Science & Engineering C 102 (2019) 708–717

Contents lists available at ScienceDirect

Materials Science & Engineering C

journal homepage: www.elsevier.com/locate/msec

Bifunctional and highly sensitive electrochemical non-enzymatic glucose and hydrogen peroxide biosensor based on $NiCo_2O_4$ nanoflowers decorated 3D nitrogen doped holey graphene hydrogel

Zhiwei Lu[a], Lan Wu[a], Junjun Zhang[b], Wanlin Dai[a], Guangquan Mo[c], Jianshan Ye[a,*]

[a] School of Chemistry and Chemical Engineering, South China University of Technology, Guangzhou 510641, PR China
[b] School of Chemistry and Chemical Engineering, Guangdong Pharmaceutical University, Guangzhou 510641, PR China
[c] Department of Chemistry, School of Pharmaceutical Sciences, Guangzhou Medical University, Guangzhou 511436, PR China

ARTICLE INFO

Keywords:
Electrochemical sensor
Nitrogen doped holey graphene
$NiCo_2O_4$ nanoflowers
Non-enzymatic
Glucose
Hydrogen peroxide

ABSTRACT

In this work, a simple strategy for fabricating a 3D nitrogen doped holey graphene hydrogel decorated with $NiCo_2O_4$ nanoflowers (NHGH/$NiCo_2O_4$) via a one-pot hydrothermal method with subsequent calcination is reported for the first time. The novel NHGH/$NiCo_2O_4$ nanocomposites featured high electrical conductivity, large and accessible surface areas, abundant active sites, and excellent electrocatalytic performance. Considering the excellent catalytic activity of $NiCo_2O_4$, a sensitive and bifunctional electrochemical non-enzymatic biosensor was established for the determination of glucose and hydrogen peroxide (H_2O_2). The obtained biosensor exhibited wide linear ranges (glucose: 0.005–10.95 mM; H_2O_2: 1–510 μM) and a low detection limits (glucose: 0.39 μM; H_2O_2: 0.136 μM) in alkaline solution (S/N = 3). Excellent electrocatalytic activity of this sensor was ascribed to the synergistic effects of the hybrid structure between the $NiCo_2O_4$ nanoflowers and NHGH. Furthermore, the sensitive biosensor also exhibited high selectivity and could be applied to determine glucose in real blood samples. Taken together, the results reveal that the proposed hybrid nanocomposite could be a promising electrochemical biosensor.

1. Introduction

As glucose and hydrogen peroxide (H_2O_2) are closely related to human life and health [1], the importance of glucose and H_2O_2 detection is gradually increasing. Currently, diabetes is one of a major chronic disease that threatens to human health worldwide. Blood glucose level is a pathological indicator of diabetes. Therefore, rapid and accurate monitoring of blood glucose concentration is essential for the early detection and diagnosis of diabetes [2]. At the same time, H_2O_2 is a main by-product of several oxidative metabolic pathways in animal cells [3,4]. H_2O_2 disorders can lead to DNA damage and gene mutation, which is closely related to the occurrence of various diseases, e.g. cancer and cerebrovascular diseases [5]. Therefore, quantitative detection of glucose and H_2O_2 is of great significance for the effective control of some diseases and biomedical research.

In life science and basic research, increasing demands for simple, fast, sensitive, and reliable analytical methods to detect H_2O_2 and glucose. It is known that many methods have been developed for detecting glucose and H_2O_2, e.g. fluorimetry [6], chemiluminescence [7,8], and electrochemical method [9]. Of these methods, the electrochemical method is regarded as the most promising because of its practicality, high sensitivity, and low cost [10–15]. To date, numerous electrochemical enzyme immobilization biosensors based on glucose oxidase and horseradish peroxidase have been fabricated for glucose and H_2O_2 detection with good selectivity and high sensitivity [16–18]. However, enzymatic biosensors are vulnerable to environmental factors and economic influences, such as temperature, pH, and high cost [19,20]. Thus, a practical, simple and inexpensive non-enzymatic biosensor is urgently needed.

Recently, several nanomaterials such as noble metals (Pt [21], Pd [2], Au [22]), metal alloys (PdAu [23]), transition metal oxide (TMO, Co_3O_4 [24], NiO [25], TiO_2 [26], Fe_3O_4 [27]), have been used to construct non-enzymatic electrodes with high electrocatalytic activity toward glucose and H_2O_2. Unfortunately, due to the inherent poor conductivity of TMOs, the performance of these bioactive molecular sensors is still restricted. To address this issue, two viable strategies have been introduced. On the one hand, the single-phase binary metal oxides with two metal cations have been developed, for example,

* Corresponding author.
E-mail address: jsye@scut.edu.cn (J. Ye).

https://doi.org/10.1016/j.msec.2019.04.072
Received 24 July 2018; Received in revised form 20 April 2019; Accepted 23 April 2019
Available online 24 April 2019
0928-4931/

$NiCo_2O_4$ has a typical spinel structure, and a features an electronic conductivity higher than those of the single component cobalt oxides and nickel oxides (at least two orders of magnitude higher) because of its multiple oxidation states [28,29]. Inspired by the inherent catalytic activity of cobalt and nickel oxide species, many researchers have studied the applications of $NiCo_2O_4$ in H_2O_2 or glucose electrochemical sensors [23,30,31]. Among its many advantages, the, controllable morphology of $NiCo_2O_4$ provides a number of catalytically active sites suitable for glucose and H_2O_2 detection and enriches the applications of this electrode material.

On the other hand, an ideal electrode materials that allow anchoring of $NiCo_2O_4$ onto some support, including porous carbon [32], graphene [33], and carbon nanotube [34], have been widely evaluated. Among them, graphene has received research attention due to its excellent electrical conductivity, large specific surface area, and high mechanical strength [35]. Interestingly, several graphene-based electrodes have been fabricated into electrochemical biosensors because the material allows extensive reagent adsorption and reaction [4]. Graphene composites hybridized with noble metals, metal oxides and macromolecules have been developed to prepare glucose or H_2O_2 electrochemical sensors with enhanced electrochemical properties [19,31,36]. Rao et al. successfully used reduced graphene oxide to prepare an electrochemical glucose sensor with admirable electrochemical properties [37]. Thus, graphene and $NiCo_2O_4$ nanoparticles could be integrated as electrode materials to fabricate biosensors. Unfortunately, graphene is prone to aggregation, which reduces the specific surface area of the resulting composite and in turn inhibits fast mass transfer; thus, inhibiting aggregation and increasing electrochemical performance are necessary endeavors when dealing with graphene sensors. According to the literature, nitrogen doping can further facilitate charge transfers with adjacent carbon atoms and suppress the electrons and holes recombination [38,39]. Therefore, exploration of the integration of flower-like $NiCo_2O_4$ and 3D nitrogen doped holey graphene hydrogel (NHGH) for electrochemical biosensors is meaningful. To the best of our knowledge, 3D flower-like $NiCo_2O_4$ nanomaterials decorated on a 3D NHGH surface to produce a for the non-enzymatic biosensor for glucose and H_2O_2 multi-functionally detection have not yet to be reported.

In this work, a bifunctional electrochemical non-enzymatic glucose and H_2O_2 biosensor was fabricated from 3D NHGH and $NiCo_2O_4$ nanoflowers nanoflower hybrids via a simple one-pot and one-step hydrothermal process (Scheme 1). Three-dimensional flower-like $NiCo_2O_4$ not only provides a large specific surface area but also electrocatalyzes glucose and H_2O_2 oxidation. Owing to its unique morphology, 3D NHGH can solve the aforementioned problem of aggregation. The synergistic effects of 3D NHGH and $NiCo_2O_4$ nanoflowers endowed the resulting nanocomposites with excellent catalytic activity, and resulting non-enzymatic NHGH/$NiCo_2O_4$/glassy carbon electrode (GCE)-based biosensor exhibited excellent selectivity, long-term stability, and good reproducibility for glucose and H_2O_2 oxidation.

2. Experimental section

2.1. Materials and reagents

All aqueous solutions were prepared using ultrapure water (18.25 MΩ·cm). Graphite powder, Nickel (II) chloride tetrahydrate ($NiCl_2{\cdot}6H_2O$), Cobalt (II) acetate tetrahydrate [$Co(CH_3COO)_2{\cdot}4H_2O$], polyvinylpyrrolidone (PVP, K30), ethylene glycol ($C_2H_6O_2$), L-glycine ($C_2H_5NO_2$), glucose ($C_6H_{12}O_6$), hydrogen peroxide (H_2O_2, 30%), sodium hydroxide (NaOH), dopamine (DA), ascorbic acid (AA), and uric acid (UA) were purchased from Aladdin Biochemical Technology Co., Ltd. (Shanghai, China http://www.aladdin-e.com/). All of the reagents used were of analytical grade and used as received without further purification.

2.2. Synthesis of 3D flower-like $NiCo_2O_4$ decorated N-doped holey graphene hydrogel (NHGH)

Firstly, graphene oxide (GO) was synthesized via a Hummer's method, with some modifications, as described in detail in a previous work [40]. A 3D flower-like $NiCo_2O_4$ decorated N-doped holey graphene hydrogel (NHGH/$NiCo_2O_4$) was synthesized via a one-pot and one-step hydrothermal process followed by calcination. Briefly, 10 mL of H_2O_2 (30%), 2.5 mL of HCl and 100 mg of glycine were added sequentially to 40 mL of an aqueous dispersion of GO (3.2 mg/mL) under sonication for 2 h to obtain homogeneous suspension A. Co $(CH_3COO)_2{\cdot}4H_2O$ (1.0 g), $NiCl_2{\cdot}6H_2O$ (2.38 g), and PVP (0.03 g) were dissolved in 40 mL of ethylene glycol and stirred together for 1 h to obtain homogeneous mixed solution B. Then, solution A was added to solution B. After continuous ultrasonication for 30 min, the mixed solution was transferred to a Teflon-lined stainless steel autoclave for hydrothermal reaction at 180 °C for 12 h. The obtained products were filtered, washed several times with ethanol and water to remove the unreacted chemicals followed by flash-frozen with liquid nitrogen and freeze-dried. Finally, the precursor was calcined at 300 °C for 2 h to obtain 3D NHGH/$NiCo_2O_4$. For comparison, NHGH was also prepared under the same conditions but without solution B, and the pure 3D flower-like $NiCo_2O_4$ was synthesized without solution A.

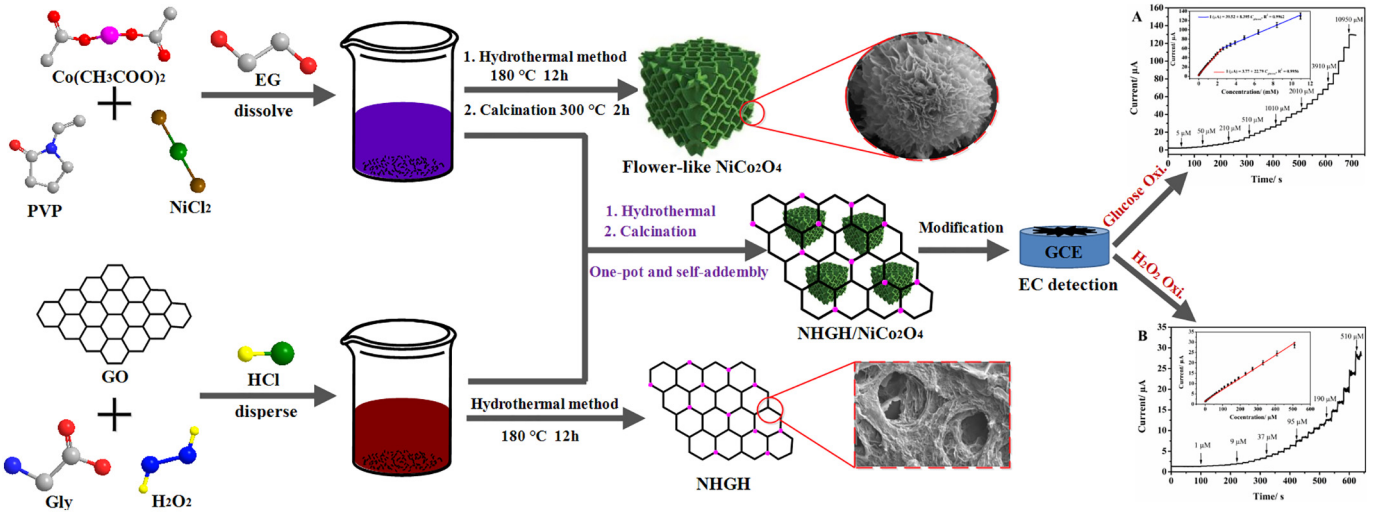

Scheme 1. Schematic illustration of the formation of the NHGH/$NiCo_2O_4$ catalysts and the bifunctional electrochemical non-enzymatic glucose and H_2O_2 sensing.

2.3. Structural characterization

The morphologies of $NiCo_2O_4$, NHGH, and 3D NHGH/$NiCo_2O_4$ were investigated via transmission electron microscopy (TEM, JEOL, JEM-2100F) and scanning electron microscopy (SEM, JEOL JSM 7500) with energy dispersive X-ray spectroscopy (EDX) mapping. X-ray diffraction (XRD) patterns were collected by a Bruker diffractometer (D8 Advance, Germany) with a Cu-Kα radiation (λ = 0.1548 nm). The Raman spectra were collected using a Jobin Yvon LabRAM Aramis spectrometer with a 532-nm laser source (H.J.Y, Ltd., France). N_2 adsorption/desorption isotherms were calculated by Quantachrome volumetric physisorption analyzer. (Autosorb-1, 77K, America). Thermogravimetric analyses (TGA) was conducted at a heating rate of 10 °C·min^{-1} under oxygen atmosphere (Netzsch TG-209 F3, Germany). X-ray photoelectron spectroscopy (XPS) spectra were collected on an ESCALAB 250Xi spectrometer (K-Alpha, Thermo Fisher Scientific, USA) with a monochromated Al Kα source (1486.6 eV).

2.4. Electrochemical measurements

All the electrochemical performance measurements, such as cyclic voltammetric (CV) and amperometric i-t curve were performed on an IGS 6030 electrochemical workstation (Guangzhou ingsens sensor Technology Co., Ltd., China http://www.ingsens.com/) using a three-electrode system, containing a bare GCE or modified GCE based working electrode, a platinum wire counter electrode, and a saturated Ag/AgCl reference electrode. 0.1 M NaOH as supporting electrolyte. The amperometric response of the NHGH/NiCo2O4/GCE to the glucose and H_2O_2 were carried out at an applied potential of 0.5 V in stirring condition.

2.5. Real samples

The human serum samples were obtained from the hospital on campus. All experiments were performed in compliance with the relevant laws and institutional guidelines.

3. Results and discussion

3.1. Characterization of NHGH/$NiCo_2O_4$

The synthetic strategy of NHGH/$NiCo_2O_4$ is schematically illustrated in Scheme 1. In this work, NHGH/$NiCo_2O_4$ was prepared via a simple one-pot hydrothermal method and subsequently calcination process. PVP acts as a stabilizer and morphology-directing reagent for the self-assembly process, and glycine served as the nitrogen source [19]. During the hydrothermal process at high temperatures, GO loses its functional groups and is reduced to nitrogen-doped reduced graphene oxide. Meanwhile, it can also be self-assembled into hydrogels with interconnected 3D porous networks structure due to the increase in the π-π stacking interactions between GO sheets [41]. At the same time, H_2O_2 molecules can partially oxidize and etch the carbon atoms in GO to generate carbon vacancies, eventually forming some nanopores structure. On the other hand, ethylene glycol as a reaction solvent can limit the nucleation process, undergoes nucleation-growth-crystallization to finally form flower-like $NiCo_2O_4$ under PVP protection [42].

The surface morphologies of the NHGH, pure $NiCo_2O_4$, and NHGH/$NiCo_2O_4$ were characterized using SEM (Fig. 1). A 3D graphene framework with interconnected pores and porous structures can be clearly observed in Fig. 1a. Fig. 1b exhibits the uniformly dispersed 3D flower-like architecture of $NiCo_2O_4$ with an average diameter of 3 μm. After incorporation of $NiCo_2O_4$ into NHGH, the presence of $NiCo_2O_4$ nanoflowers can be clearly observed within the 3D NHGH network (Fig. 1c). The high magnification SEM image in Fig. 1d further demonstrates the partial encapsulation of $NiCo_2O_4$ nanoflowers by NHGH. This hybrid structure of the as-prepared sample results in a large surface area and promotes mass transfer. Besides, EDS results (Fig. S1) and the elemental mappings reveal the homogenous distribution of C, N, O, Co, and Ni element in NHGH/$NiCo_2O_4$ (Fig. 1e).

The structural characteristics of as-prepared GO (curve a), NHGH (curve b), NiO (curve c), $NiCo_2O_4$ (curve d), and NHGH/$NiCo_2O_4$ (curve e) were characterized by XRD. As shown in Fig. 2A, the sharp peaks at 2θ = 10.5°, and 25.4°, which confirmed the presence of the typical C (002) and C (100) planes of the graphene sheets, respectively [33]. Compared with the XRD pattern of GO, that of NHGH showed two broad peaks with poor ordering along their stacking direction at 23.6° and 45.8°. During the hydrothermal process, elimination of functional groups decrease the interlayer spacing of the NHGH, which means NHGH is composed of few-layered stacked graphene sheets, consistent with the SEM results. Peaks at 2θ = 18.9°, 31.3°, 36.7°, 44.5°, 59.1°, and 64.9° can be indexed to the (111), (220), (311), (400), (511), and (400) crystal planes of the face-centered cubic (*fcc*) structure of $NiCo_2O_4$ (JCPDS No. 20-0781), respectively [42,43]. However, except for $NiCo_2O_4$, not obvious characteristic peaks of graphene were observed in NHGH/$NiCo_2O_4$, which could be ascribed to the strong peak intensity of $NiCo_2O_4$ and the low graphene content of the hybrid. In addition, the diffraction peaks of NiO were not observed in curve e, which indicates that NHGH/$NiCo_2O_4$ composite was successfully prepared. For comparison, the XRD patterns and SEM images of the NHGH/NiO and NHGH/$NiCo_2O_4$ samples (Fig. S2A) are discussed in the Supporting Information, which indicate that the NHGH/NiO and NHGH/$NiCo_2O_4$ were successfully fabricated.

The crystal phases of the NHGH/$NiCo_2O_4$ were also characterized by Raman spectroscopy, as shown in Fig. 2B. It is clear that all the samples consist of two prominent peaks at 1334 cm^{-1} for the D band and 1593 cm^{-1} for the G band, respectively. In general, the G band arises from the first-order scattering of the E_2g mode, while the D band is associated with structural defects on the carbon basal plane. The ratio of the intensities of the D and G band (I_D/I_G) is a measure of the amount of disorder present within the carbon material [33,44]. The I_D/I_G ratios of the samples in this study showed the order GO (1.028) < NHGH/$NiCo_2O_4$ (1.049) < NHGH (1.140), which indicates the formation of new quasi-amorphous sp^2 bonded carbons during the hydrothermal process, and the incorporation of $NiCo_2O_4$ introduced more defects into the NHGH [33]. Besides, both D and G band of NHGH/$NiCo_2O_4$ exhibits a small red shift compared with that of GO, suggesting a potential interaction between graphene and $NiCo_2O_4$.

The physical properties of the NHGH/$NiCo_2O_4$ nanocomposites were determined by measuring their N_2 adsorption–desorption isotherms. As depicted in Fig. 2C, a typical IV isotherm (IUPAC classification) with a hysteresis loop extending in the relative pressure were observed, which implies the coexistence of both micro- and mesoporous structures in the NHGH/$NiCo_2O_4$ composites. The surface area of all samples was analyzed by the Brunauer–Emmett–Teller (BET) method, and the results are-summarized in Table 1. The specific surface area of pure $NiCo_2O_4$ (61.25 $m^2 \cdot g^{-1}$) with a pore size of 2.77 nm was similar to that reported a previous study [45]. The specific surface area of NHGH/$NiCo_2O_4$ determined by the BET method was 577.3 $m^2 \cdot g^{-1}$ and the composite revealed a narrow pore size of 0.69 nm, which is 9.43 times and 3.13 times higher than those of pure $NiCo_2O_4$ and NHGH, respectively. In addition, NHGH/$NiCo_2O_4$ (577.3 $m^2 \cdot g^{-1}$) exhibited a surface area larger than that reported for pure $NiCo_2O_4$ nanowires (51 $m^2 \cdot g^{-1}$), and GO-$NiCo_2O_4$ (125 $m^2 \cdot g^{-1}$), as well as $NiCo_2O_4$@GO (86 $m^2 \cdot g^{-1}$) [45]. Such a large surface area can be attributed to the improvements in dispersion endowed by the porous nitrogen-doped graphene to $NiCo_2O_4$ and increases in NHGH sheets spacing due to the introduction of the 3D flower-like structure of $NiCo_2O_4$.

The thermal stability of the nanomaterials was further investigated by TGA (Fig. 2D). The initial weight loss occurring below 100 °C is ascribed to desorption of physically adsorbed water molecules. Compared with the $NiCo_2O_4$ samples, a rapid weight loss in the range of 300–400 °C was observed for NHGH/$NiCo_2O_4$, which is due to the

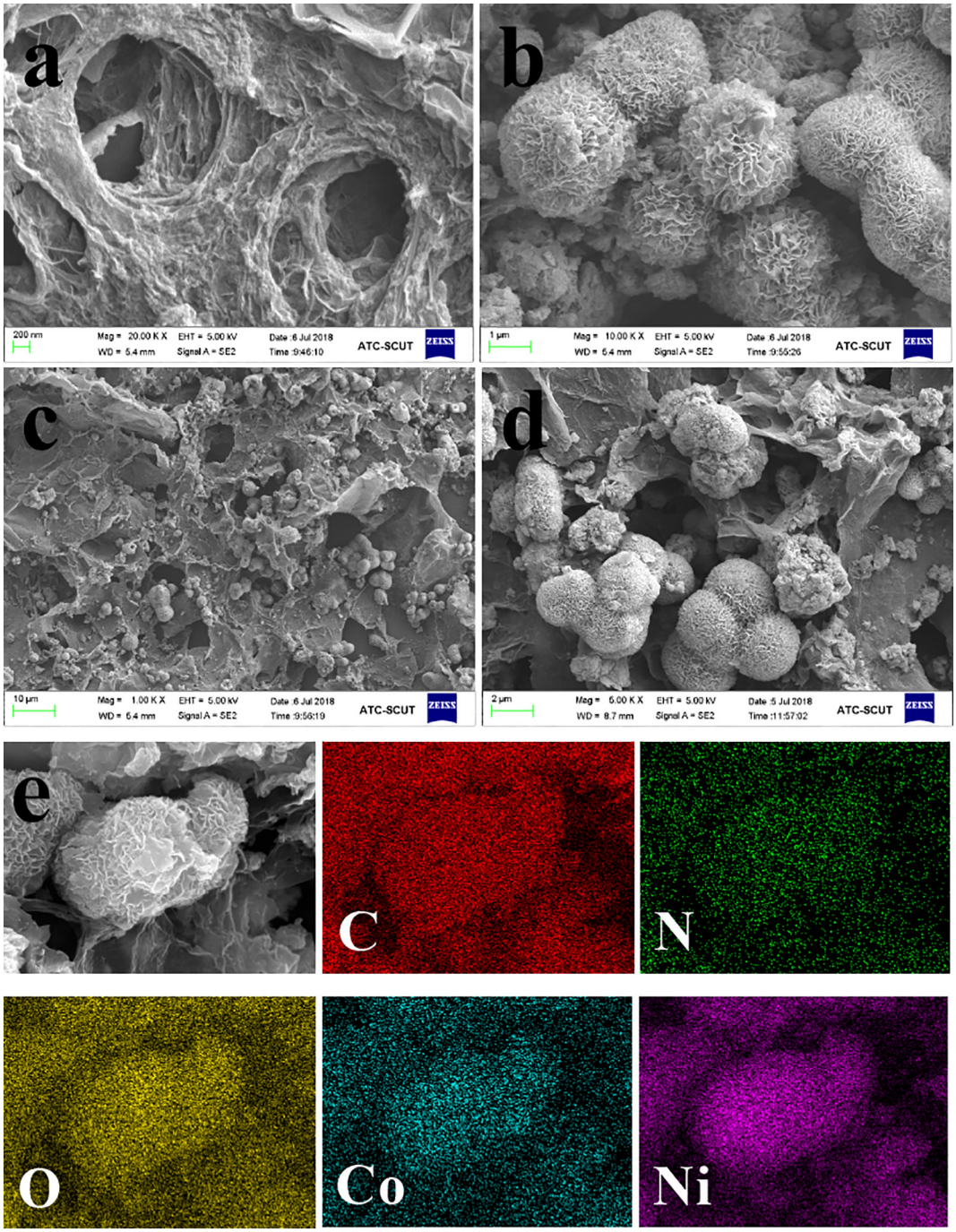

Fig. 1. SEM images of (a) NHGH, (b) pure $NiCo_2O_4$, (c–e) NHGH/$NiCo_2O_4$, and the corresponding elemental mapping of C, N, O, Co, and Ni element.

decomposition of functional groups of HNGH. Moreover, the major weight loss in the range of 450–500 °C is attributed to the partial decomposition of $NiCo_2O_4$ crystals, resulting in the emergence of NiO [30]. Whereas, the abrupt weight loss in the range of 700–800 °C is most likely due to the decomposition of the carbon skeleton of the NHGH framework.

The chemical composition of NHGH/$NiCo_2O_4$ was investigated by XPS analysis. XPS full scan survey spectrum obtained further confirmed the presence of C, N, O, Co, and Ni in NHGH/$NiCo_2O_4$ (Fig. 3A). Moreover, the measured N content reached 3.0%. Obviously, four individual peaks could be clearly observed in the high-resolution N 1s spectrum (Fig. 3B), which could be assigned to pyridinic N (398.8 eV), pyrrolic N (399.8 eV), graphitic N (401.5 eV), and oxidized N (403.8 eV), respectively [33]. Besides, the high-resolution C 1 s spectrum showed four peaks are attributable to 284.6 eV (C-C/C = C), 285.6 eV (C-O/C-N), 286.2 eV (C=O), and 288.1 eV (O-C = O), respectively (Fig. S3A) [46]. It is indicated that glycine as the nitrogen source causes nitrogen atoms were doped into the graphene lattice successfully, and four nitrogen species were formed within NHGH. The high-resolution Ni 2p spectrum shown in Fig. 3C exhibits two spin-orbit doublets belong to Ni^{2+} (856.9 eV) and Ni^{3+} (873.70 eV) ions, respectively. Whereas, another two shake-up satellite peaks (identified as "Sat.") are observed that comprised mixture of both Ni^{2+} and Ni^{3+} [47]. Similarly, in the Co 2p spectrum (Fig. 3D), two types of spin-orbit doublet peaks for Co^{2+} and Co^{3+} and two shake-up satellite peaks could be observed [34]. Based on the above analysis, the presence of the solid-state redox couples (Ni^{2+}/Ni^{3+} and Co^{2+}/Co^{3+}), and the N-doped holey graphene can offer rich electroactive sites for glucose

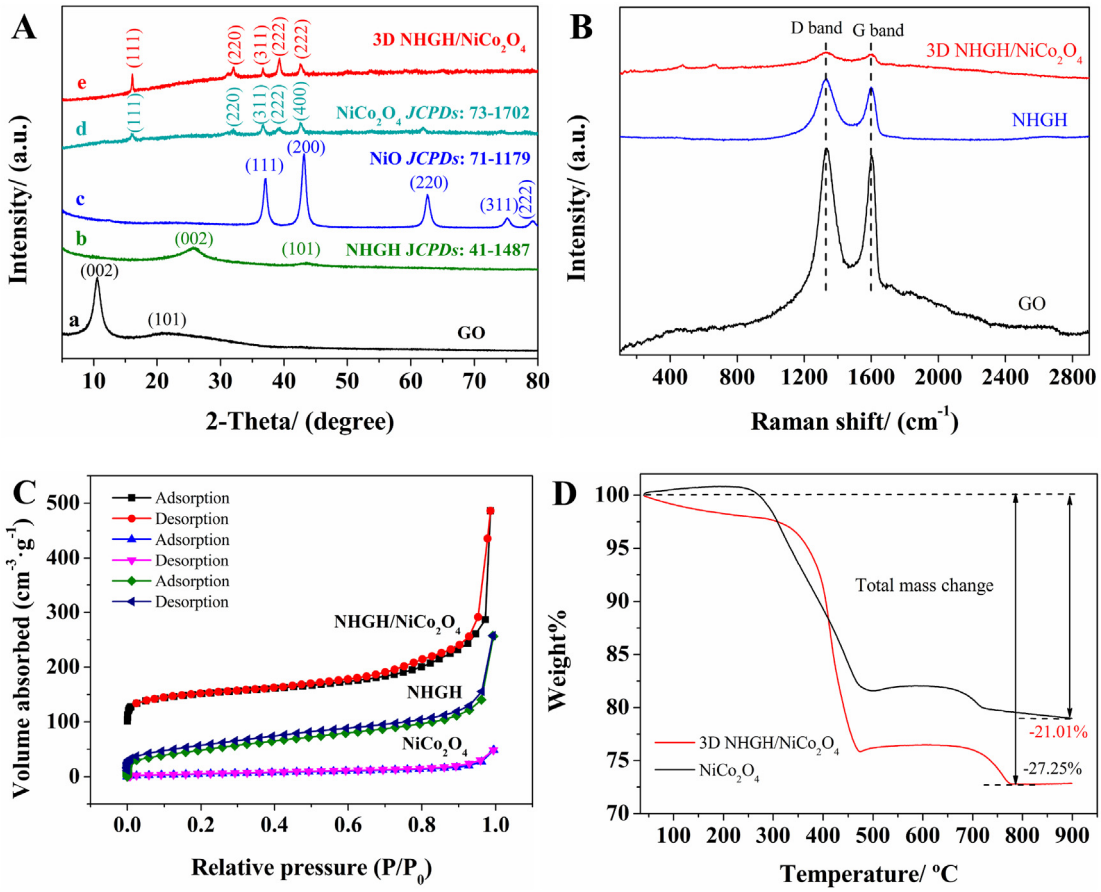

Fig. 2. Samples characterization. (A) XRD patterns, (B) Raman spectra, (C) N_2 adsorption-desorption isotherms and (D) TGA curves of the as-prepared samples.

Table 1
BET special surface area of pure $NiCo_2CO_4$, NHGH and NHGH/$NiCo_2CO_4$ samples.

Samples	S_{BET} ($m^2 \cdot g^{-1}$)	d_{DFT}
$NiCo_2CO_4$	61.25	2.77
NHGH	184.7	0.54
NHGH/$NiCo_2CO_4$	577.3	0.69

Brunauer-Emmet-Teller surface area (SBET) calculated at $P/P_0 = 0.99$; Pore size derived from the nonlocal density functional theory (NLDFT) method in Fig. S2B.

oxidation. These features may be important factors contributing to the notable electrocatalytic performance of spinel $NiCo_2O_4$ microspheres.

3.2. Electrocatalytic behavior of the modified electrodes

The electrochemical catalytic performances of different electrodes for glucose oxidation were investigated by cyclic voltammetry in 0.1 M NaOH solution. Fig. 4A displays the cyclic voltammograms (CVs) of these electrodes. Compared with the weak anodic peak current of bare GCE, the enhanced oxidation peak current of NHGH at 0.5 V is mainly attributed to its enlarged surface area and good conductivity. However, $NiCo_2O_4$/GCE exhibited a distinct pair of redox peaks, which indicates that the electrochemical activity of $NiCo_2O_4$/GCE is much higher than those of bare GCE and NHGH/GCE. Such features may be ascribed to the redox reactions of Co and Ni species in the alkaline electrolyte, similar to findings in the previous reports. The relevant mechanisms are described in the following equations [48]:

$$NiCo_2O_4 + OH^- + H_2O \rightarrow NiOOH + 2CoOOH + e^- \quad (1)$$

$$CoOOH + OH^- \rightarrow CoO_2 + H_2O + e^- \quad (2)$$

Besides, the potential of the oxidation peak of the NHGH/$NiCo_2O_4$/GCE was negatively shifted by 63 mV compared with that of the $NiCo_2O_4$/GCE, indicating that the conductivity of the former is better than that of the latter. However, compared with the $NiCo_2O_4$/GCE, NHGH/$NiCo_2O_4$/GCE exhibited slightly comparable electrochemical activity with the onset potential positive than 0.4 V.

Fig. 4B shows the electrochemical catalytic performance of different electrodes toward glucose oxidation in 0.1 M NaOH electrolyte. Upon addition of 5.0 mM glucose, the NHGH/$NiCo_2O_4$/GCE exhibited a single forward glucose oxidation peak current with a positive onset potential than 0.3 V and the highest peak current at 0.5 V than that of other modified electrodes. The enhancement in peak current clearly demonstrates that the NHGH/$NiCo_2O_4$/GCE is better able to catalyze glucose oxidation than bare GCE or NHGH/GCE, possibly due to the synergistic effect of $NiCo_2O_4$ and NHGH. Then, as the glucose concentration increased, it can be clearly observed that the glucose oxidation current increases at the potential of approximately 0.5 V (Fig. S4). These results demonstrate that NHGH/$NiCo_2O_4$ composites possess excellent catalytic performance for glucose oxidation. The negative shift of the peak potential and the increased peak current for oxidation of glucose may be due to the kinetic effect of an increase in the electroactive surface and the electron transfer ability of the modified electrode. Besides, the peak current of this sensor in the presence of glucose is better than that in the absence of glucose, and the catalytic mechanism for glucose electro-oxidation on $NiCo_2O_4$ can be briefly described as follows: [49].

$$NiCO_2O_4 + OH^- + H_2O \rightarrow NiOOH + 2CoOOH + e^- \quad (3)$$

$$NiOOH + glu\cos e \rightarrow Ni(OH)_2 + glucolactone \quad (4)$$

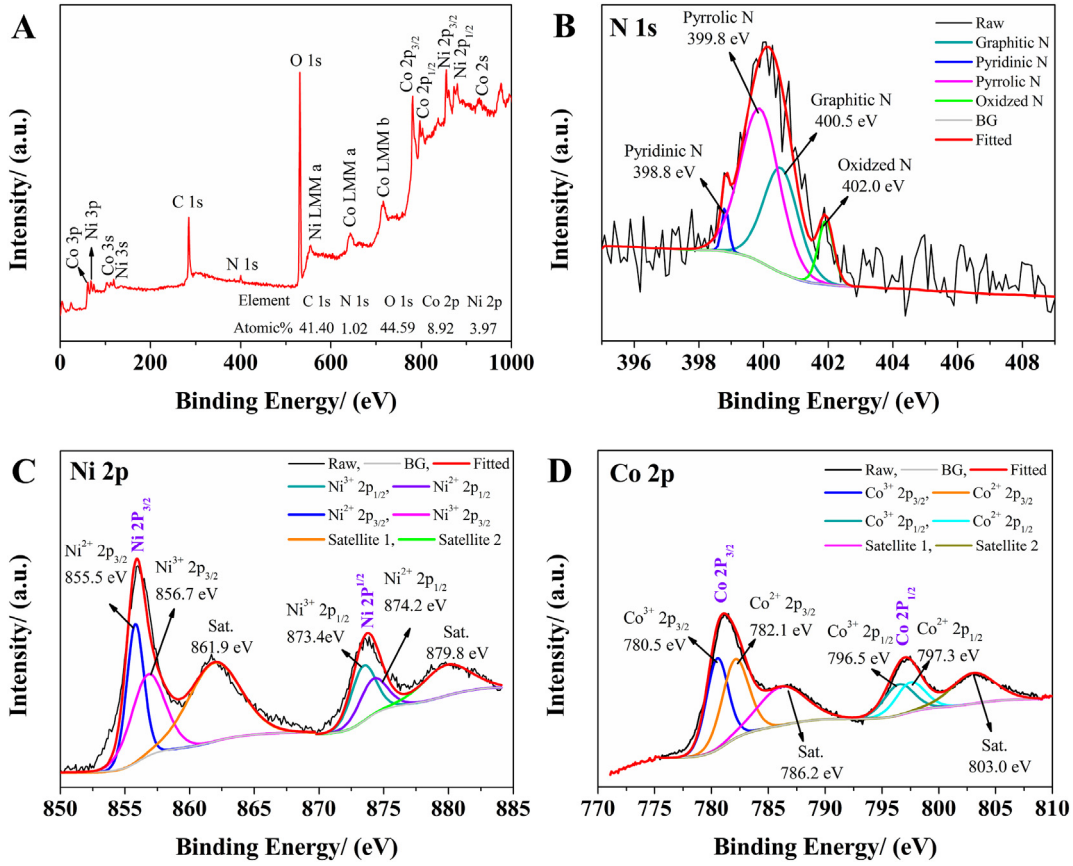

Fig. 3. XPS spectrum of NHGH/$NiCo_2O_4$ composites. (A) full scan survey; High-resolution N 1s (B), Co 2p (C), and Ni 2p (D) spectrum.

$$2CoOOH + 2glu\cos e \rightarrow 2Co(OH)_2 + 2glucolactone \quad (5)$$

In alkaline media, $NiCo_2O_4$ tends to be oxidized to NiOOH and CoOOH species (Eq. (3)). When in the presence of glucose, the glucose molecules can be rapidly catalytically oxidized into gluconolactone by NiOOH and CoOOH species, while Ni^{3+} and Co^{3+} were reduced to Ni^{2+} and Co^{2+} at the same time, respectively (Eqs. (4) and (5)) [37,48].

The electrochemical kinetics of the NHGH/$NiCo_2O_4$/GCE was evaluated under different scan rates ranging from 20 mV·s^{-1} to 200 mV·s^{-1} in 0.1 M NaOH solution containing 2.5 mM glucose. It can be seen that as the scan rate increases, the glucose oxidation peak currents gradually increased (Fig. 4C). Moreover, both the anodic and cathodic peak currents were linearly correlated with the square root of the scan rate, and the correlation coefficient (R^2) were found to be 0.9966 and 0.9999, respectively. These results imply that the electrochemical oxidation of glucose is a typical surface-controlled electrochemical process [50]. Besides, the calculation method for the electroactive surface area of the modified electrodes based on the Randles-Sevcik equation is described in the Supporting Information. The electroactive surface area of NHGH/$NiCo_2O_4$ was increased by 23.60%, which is ascribed to the 3D hierarchical architecture of NHGH/$NiCo_2O_4$ nanocomposites (Fig. S5).

3.3. Sensing performance for glucose detection

During electrochemical determination process, the appropriate working potential is an important parameter for obtaining high sensitivity. Fig. S6 displays a series of stepped amperometric responses obtained from the 3D NHGH/$NiCo_2O_4$/GCE with successive addition of 0.1 mM glucose at various potentials from 0.45 V to 0.55 V. The currents increments with the increasing of the applied potential until the potential reached +0.5 V, but the currents increments began to decline at +0.55 V. Considering the effect of water oxidation at high potential, +0.5 V was chosen as the optimal potential with which to evaluate the performance of the sensor. As expected, the peak currents linearly increased with the concentration increasing (Fig. 5A). The steady-state current responses were achieved within 4 s, indicating that the 3D NHGH/$NiCo_2O_4$ composites have good electrocatalytic properties and rapid electron exchange performance. The 3D NHGH/$NiCo_2O_4$-based sensor exhibited a wide linear relationship between peak current and glucose concentration in the range of 5 μM–2.6 mM and 2.6 mM–10.9 mM, respectively (Fig. 5B). The linear regression equations are I (μA) = 22.79$C_{glucose}$ (mM) + 3.77 (R^2 = 0.9956) and I (μA) = 8.395$C_{glucose}$ (mM) + 39.52 (R^2 = 0.9962), respectively. The sensitivity of the sensor was about 2072 μA·mM^{-1}·cm^{-2}, and its limit of detection (LOD) was 0.39 μM [S/N = 3], which demonstrates the 3D NHGH/$NiCo_2O_4$/GCE has a high sensitivity and a wide linear range for glucose detection. Compared with previous reports on glucose determination in 0.1 M NaOH electrolyte (Table 2), the proposed sensor shows better sensitivity, a wider linear range, and faster response times than $NiCo_2O_4$@PANI and pure $NiCo_2O_4$ microspheres. These properties are ascribed to the fact that the presence of N-doped holey graphene and flower-like $NiCo_2O_4$, which can greatly increase the availability of electrocatalytic active areas and accelerate electron transfer during glucose oxidation.

Newly-designed 3D NHGH/$NiCo_2O_4$ hydrogel has several important merits: (1) 3D flower-like structure can offer a significantly large specific surface areas and increase the contact areas at the electrode/electrolyte interface for facilitate the mass transfer at interfaces, as well as provide more active sites for electrochemical catalysis reactions; (2) nitrogen doped porous graphene hydrogel will enable an efficient electron transport path; (3) uniformly dispersed $NiCo_2O_4$ with a tunable morphology can greatly enhance the catalytic binding sites of glucose

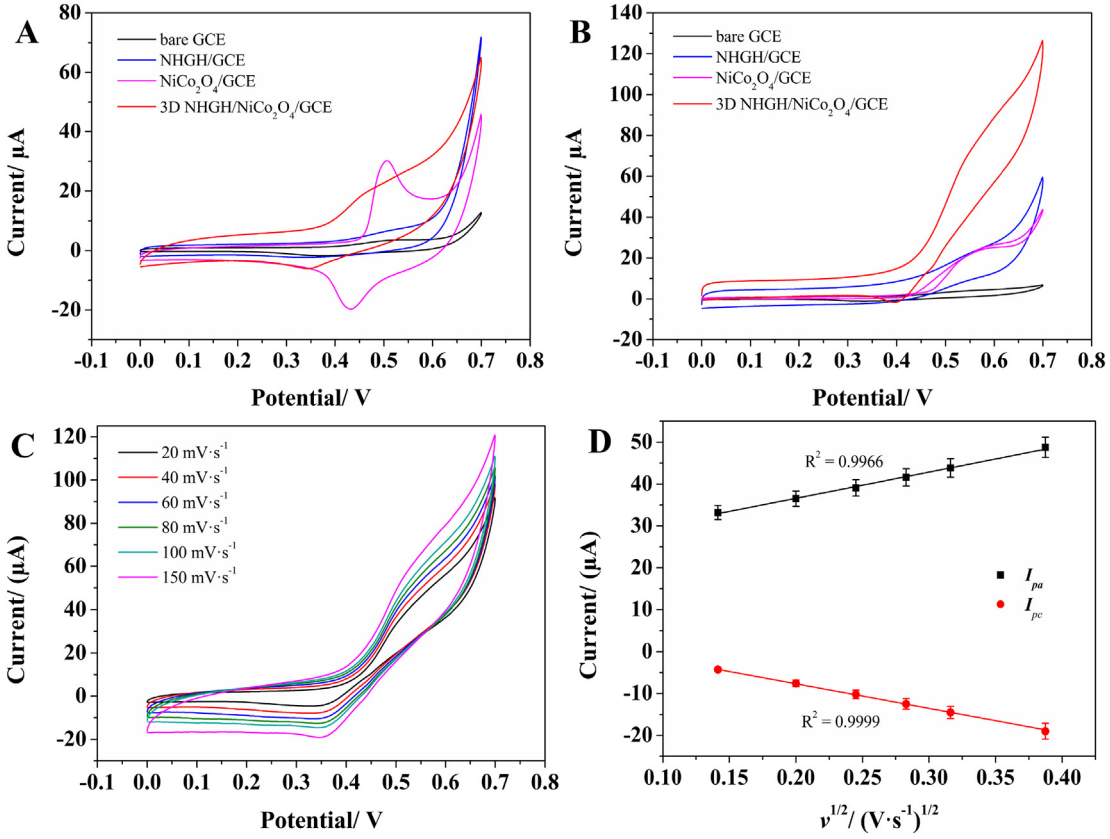

Fig. 4. Cyclic voltammetry (CV) curves of bare GCE, NHGH/GCE, $NiCo_2O_4$/GCE, and NHGH/$NiCo_2O_4$/GCE in the absence (A) and in the presence (B) of 5 mM glucose in 0.1 M NaOH solution with a scan rate of 50 mV·s^{-1}. (C) CV curves of 3D NHGH/$NiCo_2O_4$ modified electrode in 0.1 M NaOH solution containing 5 mM glucose at different scan rates, and (D) is the corresponding calibration curves.

molecules.

3.4. Selectivity, reproducibility and stability of the 3D NHGH/$NiCo_2O_4$ sensor and real sample analysis

Considering that some electroactive biological molecules, such as ascorbic acid (AA), uric acid (UA), and dopamine (DA), coexist with glucose in human blood, these molecules may interfere with the actual determination of glucose. In general, the physiological concentration of glucose is usually 10 times higher than that of the interfering species [19]. Therefore, 5 mM glucose, 0.5 mM DA, 0.5 mM AA, 0.5 mM UA, and 2.5 mM glucose were successively added into 0.1 M NaOH solution for interference experiments. No obviously oxidation current changes were observed (Fig. 6A), thereby confirming that the excellent selectivity of the as-prepared sensor for glucose. Such selectivity can be ascribed to the electrostatic repulsion between anions of the biological molecules (DA, UA, and AA) and the negatively charged sulfonic groups of Nafion film. The reproducibility of the sensors was investigated by comparing the response currents of seven modified electrodes toward 2.5 mM glucose. The relative standard deviation (RSD) of current response for seven modified electrodes was 8.35%, and the repeatability of one sensor was 5.27% for ten measurements for the same electrode under the same condition. After 4000 s chronoamperometric response of 3D NHGH/$NiCo_2O_4$/GCE sensor in 5 mM glucose solution, the

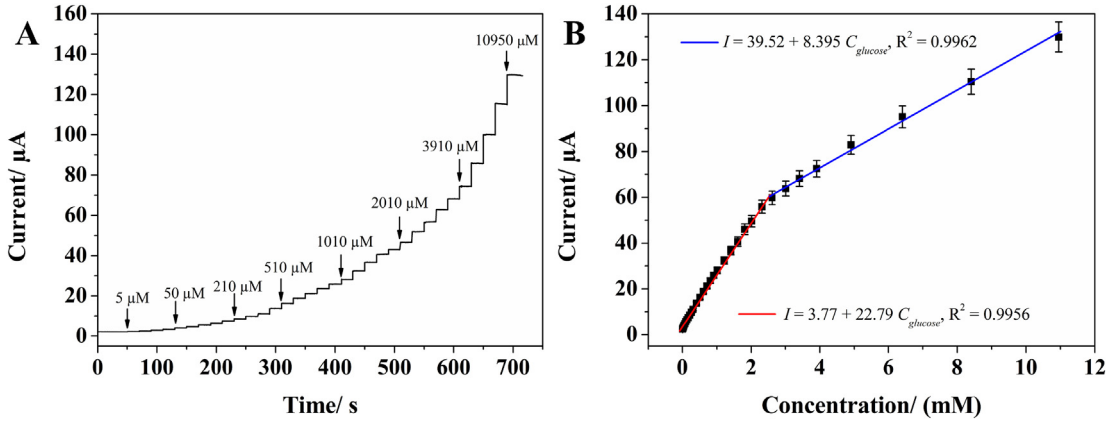

Fig. 5. (A) Amperometric response of 3D NHGH/$NiCo_2O_4$/GCE to the successive addition of glucose at regular intervals and (B) the corresponding calibration curve. The experiment was carried out at 0.5 V in the stirred 0.10 M NaOH solution.

Table 2
Comparison of non-enzymatic electrochemical glucose sensors in 0.1 M NaOH solution.

Electrode materials	Response time (s)	Sensitivity ($\mu A \cdot mM^{-1} \cdot cm^{-2}$)	Linear range (mM)	Detection limit (μM)	Working potential (V)	Ref.
Co_3O_4 nanofibers	7	36.25	Up to 2.04	0.97	+0.59	[51]
Co_3O_4 NF/GOH	8	537.4	0.25–10.00	N.A	+0.62	[19]
c-$Ni(OH)_2$ HR	10	1569	0.002–3.862	0.6	+0.60	[50]
$NiCo_2O_4$@PANI	5	4550	0.015–4.735	0.38	+0.50	[49]
$NiCo_2O_4$ microspheres	8	430.86	0.01–10.48	N.A	+0.55	[30]
NHGH/$NiCo_2O_4$	4	2072	0.005–10.95	0.39	+0.50	This work

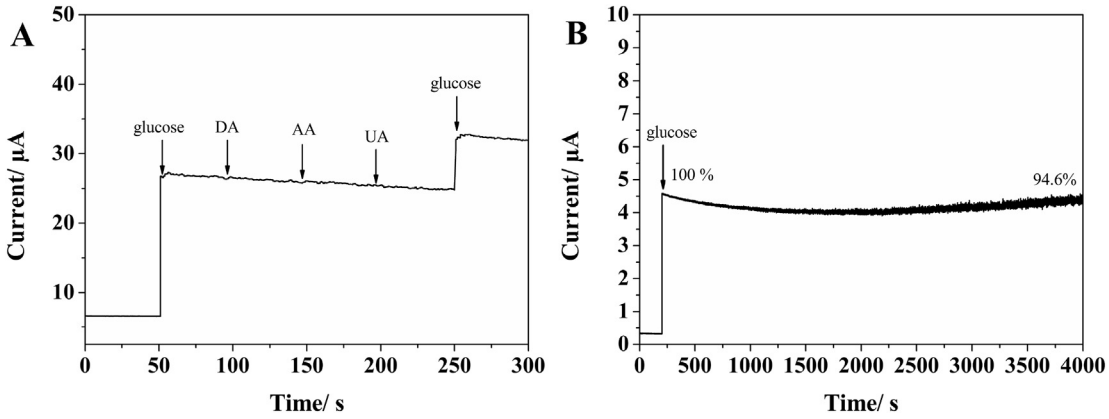

Fig. 6. (A) Amperometric response of 3D NHGH/$NiCo_2O_4$/GCE to the successive addition of 5 mM glucose, 0.5 mM DA, 0.5 mM AA, 0.5 mM UA, and 2.5 mM glucose (B) i-t plot of NHGH/$NiCo_2O_4$/GCE recorded in the presence of 1 mM glucose. All the experiments were carried out at 0.5 V in the stirred 0.10 M NaOH solution.

Table 3
Comparison of the results of glucose detection in human serum samples by NHGH/$NiCo_2O_4$/GCE and the commercial glucose meter.

Samples	Glucose sensor in this work (mM)	Results from hospital (mM)	Commercial glucose meter (mM)	Recovery%
1	7.96	8.13	8.35	97.9
2	6.85	6.99	7.08	98.0
3	7.41	7.23	7.16	102.5
4	6.52	6.47	6.50	100.8

oxidation peak current was maintained at 94.6% relative to the initial current value. Besides, the current response of NHGH/$NiCo_2O_4$/GCE sensor to 2.5 mM glucose was still remained at 92.5% of the original current value after storage in a refrigerator at 4 °C conditions for four weeks. These findings reflect the good stability of the modified electrode and ensure high accuracy during glucose detection. Finally, in order to verify the practical application of NHGH/$NiCo_2O_4$/GCE, it was applied to determine glucose in human blood serum via the standard addition method. 20 μL of blood serum was mixed with 10 mL of 0.1 M NaOH solution and the current response of this mixture was measured at a working potential of +0.5 V. Thereafter, standard solutions of glucose were injected into the mixed solution at 20 s intervals and the increase in currents was recorded. The amount of glucose in the serum sample was calculated from the calibration curve (Fig. 5B). The experiments results are listed in Table 3. The results showed that the concentration of glucose measured by the NHGH/$NiCo_2O_4$/GCE was consistent with that measured by a commercial glucose meter, thus proving the feasibility of NHGH/$NiCo_2O_4$/GCE as an accurate and reliable non-enzymatic sensor for detecting glucose in biological samples.

3.5. Sensing performance for H_2O_2 detection

The electrocatalytic performance of NHGH, $NiCo_2O_4$, and NHGH/$NiCo_2O_4$ for H_2O_2 detection was evaluated by CV in the presence and absence of 3 mM H_2O_2. The effects of different supporting electrolytes including 0.1 M NaOH and phosphate buffer saline (PBS) different pH (pH = 6.0/7.0) solutions were studied. The 3D NHGH/$NiCo_2O_4$/GCE exhibited low electrocatalytic activity for H_2O_2 oxidation/reduction with weak current in PBS (pH = 6.0/7.0) (Fig. 7A). However, a pair of redox peaks with high current responses was observed when detection with the NHGH/$NiCo_2O_4$-modified GCE was conducted in 0.1 M NaOH solution (Fig. 7A). This result indicates that NHGH/$NiCo_2O_4$ has excellent catalytic performance toward H_2O_2 in NaOH electrolytes solution. Compared with NHGH and $NiCo_2O_4$, 3D NHGH/$NiCo_2O_4$ exhibited higher current responses toward H_2O_2 oxidation with onset potential positive than 0.4 V. (Fig. 7B). In view of the onset potential electrochemical characteristics of anode or cathode in the reversible H_2O_2 oxidation, either positive potential or negative potential can be chosen for NHGH/$NiCo_2O_4$ electrochemical catalytic H_2O_2 [52]. Moreover, the anodic peak currents increased with increasing H_2O_2 concentration, as shown in Fig. S7. As expected in Fig. S8, both the anodic and the cathodic peak currents were linearly related to the square root of the scan rate ($v^{1/2}$), indicating that H_2O_2 undergoes a diffusion-controlled process on the NHGH/$NiCo_2O_4$/GCE, which is beneficial to quantitative detection of H_2O_2 through electrochemical means. Besides, to avoid the effects of water oxidation, the amperometric i-t curve of +0.5 V was selected for further electrochemical oxidation determination of H_2O_2 in 0.1 M NaOH solution. The calibration curve of the current response versus H_2O_2 was I (μA) = $0.0597C_{H2O2}$ (μM) + 1.411 (R^2 = 0.9945) in the range of 1–510 μM, with a detection limit of 0.136 μM (S/N = 3). Based on the above results, the mechanism of NHGH/$NiCo_2O_4$ catalyzed H_2O_2 oxidation in 0.1 M NaOH solution can be described as follows:

$$NiCo_2O_4 + OH^- + H_2O \rightarrow NiOOH + 2CoOOH + e^- \quad (6)$$

$$2NiOOH + 3H_2O_2 \rightarrow 2Ni(OH)_2 + O_2 + 2H_2O \quad (7)$$

$$2CoOOH + 3H_2O_2 \rightarrow 2Co(OH)_2 + O_2 + 2H_2O \quad (8)$$

Taking into account the O_2 generation based on the electrocatalytic oxidation toward H_2O_2, it will cause a large background noise and low

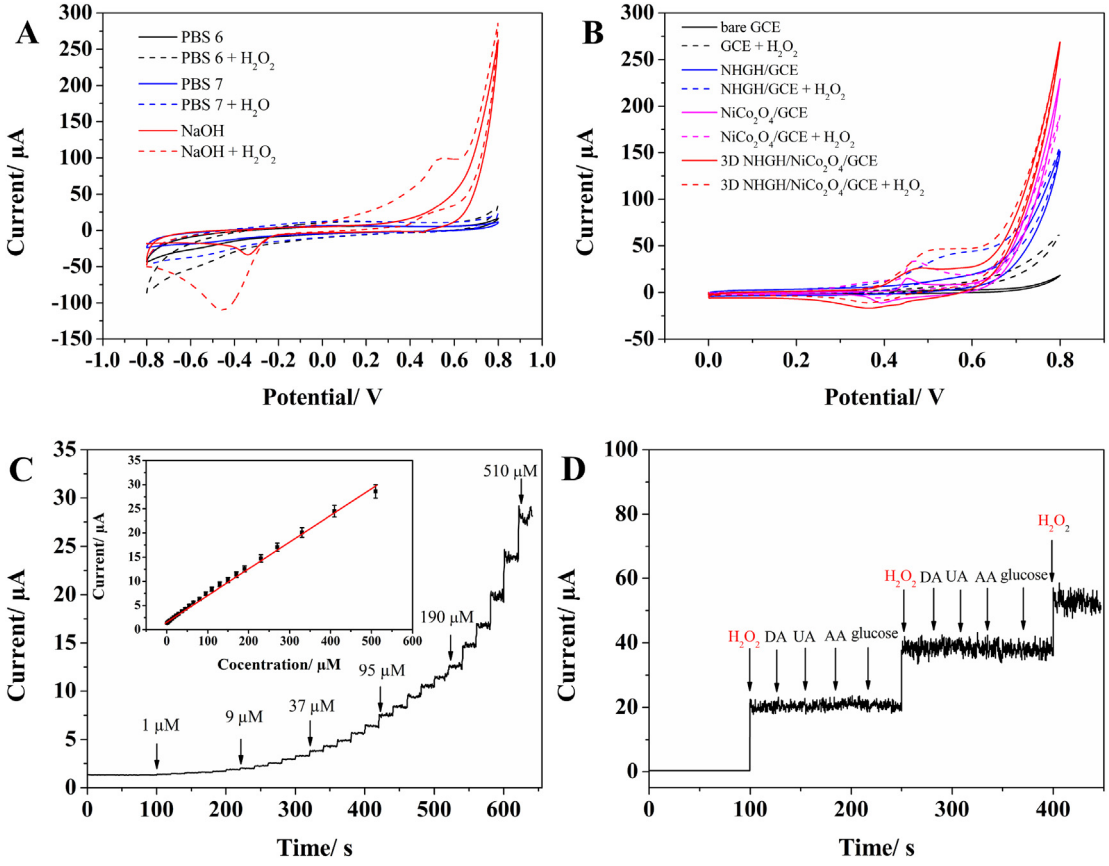

Fig. 7. (A) CVs of NHGH/$NiCo_2O_4$/GCE in the different electrolyte solution with 3 μM H_2O_2. (B) CVs of bare GCE, NHGH/GCE, $NiCo_2O_4$/GCE, and NHGH/$NiCo_2O_4$/GCE in the absence and in the presence of 5 μM H_2O_2. (C) Amperometric response of 3D NHGH/$NiCo_2O_4$/GCE in 0.1 M NaOH solution to the successive injection of different concentration of H_2O_2. (Insert: the corresponding fitting curves). (D) Amperometric responses to the successive addition of H_2O_2, DA, UA, AA, and glucose respectively on NHGH/$NiCo_2O_4$/GCE. Above experiments were carried out at 0.5 V in the stirred 0.10 M NaOH solution and the scan rate of 100 $mV \cdot s^{-1}$.

sensitivity in a high concentration of H_2O_2 (> 510 μM). Therefore, the proposed sensor in this work has a lower detection limit within the low concentration range of H_2O_2 detection. Besides, as some biologically important compounds, including DA, UA, AA, and glucose, may interfere with H_2O_2 determination, the effects of these compounds on the selectivity of the sensor were studied. Comparison of the current responses of the sensor toward H_2O_2 before and after addition the interfering substances showed no effect (Fig. 7D). Above results demonstrate that the NHGH/$NiCo_2O_4$/GCE-based sensor has a high selectivity toward H_2O_2, and, as such, may be considered a promising electrode material for detecting H_2O_2. The excellent performance of the sensor can be attributed to the following aspects: (1) flower-like $NiCo_2O_4$ provides a large specific surface, and exposes a large number of effective active catalytic sites to the electrolyte; (2) NHGH offers rapid electron transport paths between NHGH and $NiCo_2O_4$ to accelerate electron transport.

4. Conclusions

In summary, a novel bifunctional electrochemical enzyme-free biosensor based on 3D flower-like NHGH/$NiCo_2O_4$ nanocomposites was developed via a one-pot hydrothermal process with subsequent calcination for the ultrasensitive detection of glucose and H_2O_2. Given the high electronic conductivity of 3D NHGH, and the large specific surface area of the $NiCo_2O_4$ nanoflowers, as well as the rich binary electroactive sites of Co and Ni species, the newly designed NHGH/$NiCo_2O_4$/GCE revealed outstanding bifunctional electrochemical activity toward glucose and H_2O_2 detection in an alkaline solution, such as a high sensitivity, low LOD, and good selectivity. Therefore, 3D NHGH/$NiCo_2O_4$ nanocomposites could be used as a promising electrode material to fabricate biosensor. However, it should be noted that a major limitation of this sensor is its operation in strongly alkaline solution, which may hinder the determination of glucose and H_2O_2 in practical applications. Future studies will focus on developing new nanosensors that work at near-neutral pH conditions, possible through NHGH modification.

Acknowledgments

This work was supported by Science and Technology program of Guangdong Province (No. 2019B020219002, No. 2018A050506006), Guangdong Natural Science Foundation (Project No. 2017A030312005) and National Natural Science Foundation of China (NSFC, No. 21875070). We also wish to thank the engineer Qian Liu from Shiyanjia lab (www.shiyanjia.com) for help with the XPS analysis.

Appendix A. Supplementary data

Supplementary data to this article can be found online at https://doi.org/10.1016/j.msec.2019.04.072.

References

[1] A.A. Ensafi, N. Zandi-Atashbar, B. Rezaei, M. Ghiaci, M. Taghizadeh, Electrochim. Acta 214 (2016) 208–216.
[2] M. Han, S. Liu, J. Bao, Z. Dai, Biosens. Bioelectron. 31 (2012) 151–156.
[3] A.A. Ensafi, N. Zandi-Atashbar, M. Ghiaci, M. Taghizadeh, B. Rezaei, Mater. Sci. Eng. C 47 (2015) 290–297.
[4] M. Liu, R. Liu, W. Chen, Biosens. Bioelectron. 45 (2013) 206–212.
[5] Y. Ni, Y. Liao, M. Zheng, S. Shao, Microchim. Acta 184 (2017) 3689–3695.

[6] J. Chang, H. Li, T. Hou, W. Duan, F. Li, Biosens. Bioelectron. 104 (2018) 152–157.
[7] S.A. Kitte, W. Gao, Y.T. Zholudov, L. Qi, A. Nsabimana, Z. Liu, G. Xu, Anal. Chem. 89 (2017) 9864–9869.
[8] H. Li, C. Liu, D. Wang, C. Zhang, Biosens. Bioelectron. 91 (2017) 268–275.
[9] B. Huang, Y. Wang, Z. Lu, H. Du, J. Ye, Sensors Actuators B Chem. 252 (2017) 1016–1025.
[10] Z. Dan, C. Xiaoqin, W. Zao, H. Shuai, H. Xiandeng, Q. Fengli, D. Gu, A.A. M., Z. Chengbin, S. Xuping, Chem. Eur. J., 23 (2017) 5214–5218.
[11] K. Dhara, D.R. Mahapatra, Microchim. Acta 185 (2017) 49.
[12] H. Beitollahi, M. Safaei, S. Tajik, Anal. Bioanal. Chem. Res. 6 (2019) 81–96.
[13] S. Tajik, H. Beitollahi, Anal. Bioanal. Chem. Res. 6 (2019) 171–182.
[14] H. Beitollahi, H. Karimi-Maleh, H. Khabazzadeh, Anal. Chem. 80 (2008) 9848–9851.
[15] H. Beitollahi, Z. Dourandish, S. Tajik, M.R. Ganjali, P. Norouzi, F. Faridbod, J. Rare Earths 36 (2018) 750–757.
[16] M. Vázquez-González, W.-C. Liao, R. Cazelles, S. Wang, X. Yu, V. Gutkin, I. Willner, ACS Nano 11 (2017) 3247–3253.
[17] M.J. Chaichi, M. Ehsani, Sensors Actuators B Chem. 223 (2016) 713–722.
[18] L. Fang, B. Liu, L. Liu, Y. Li, K. Huang, Q. Zhang, Sensors Actuators B Chem. 222 (2016) 1096–1102.
[19] L.T. Hoa, J.S. Chung, S.H. Hur, Sensors Actuators B Chem. 223 (2016) 76–82.
[20] H. Beitollahi, M.A. Taher, M. Ahmadipour, R. Hosseinzadeh, Measurement 47 (2014) 770–776.
[21] C. Chen, R. Ran, Z. Yang, R. Lv, W. Shen, F. Kang, Z.-H. Huang, Sensors Actuators B Chem. 256 (2018) 63–70.
[22] T. Han, Y. Zhang, J. Xu, J. Dong, C.-C. Liu, Sensors Actuators B Chem. 207 (2015) 404–412.
[23] J. Wang, H. Gao, F. Sun, C. Xu, Sensors Actuators B Chem. 191 (2014) 612–618.
[24] H. Mahmoudi-Moghaddam, S. Tajik, H. Beitollahi, Food Chem. 286 (2019) 191–196.
[25] T. Marimuthu, S. Mohamad, Y. Alias, Synth. Met. 207 (2015) 35–41.
[26] S. Tajik, H. Beitollahi, P. Biparva, J. Serb. Chem. Soc. 83 (2018) 12.
[27] H. Beitollahi, F. Garkani-Nejad, S. Tajik, M.R. Ganjali, Iran. J. Pharm. Res. 18 (2019) 80–90.
[28] K.K. Naik, A. Gangan, B. Chakraborty, S.K. Nayak, C.S. Rout, ACS Appl. Mater. Interfaces 9 (2017) 23894–23903.
[29] Y. Changzhou, W.H. Bin, X. Yi, L.X. Wen, Angew. Chem. Int. Ed. 53 (2014) 1488–1504.
[30] H. Yin, T. Zhan, D. Qin, X. He, Q. Nie, J. Gong, Inorg. Nano-Met. Chem. 47 (2017) 1560–1567.
[31] Y. Ni, J. Xu, H. Liu, S. Shao, Talanta 185 (2018) 335–343.
[32] Z. Lu, J. Zhang, W. Dai, X. Lin, J. Ye, J. Ye, Microchim. Acta 184 (2017) 4731–4740.
[33] Z. Lu, W. Dai, X. Lin, B. Liu, J. Zhang, J. Ye, J. Ye, Electrochim. Acta 266 (2018) 94–102.
[34] L. Qian, L. Gu, L. Yang, H. Yuan, D. Xiao, Nanoscale 5 (2013) 7388–7396.
[35] C.O. C., N.S. T., Small, 6 (2010) 711–723.
[36] G. Ma, M. Yang, C. Li, H. Tan, L. Deng, S. Xie, F. Xu, L. Wang, Y. Song, Electrochim. Acta 220 (2016) 545–553.
[37] H. Rao, Z. Zhang, H. Ge, X. Liu, P. Zou, X. Wang, Y. Wang, New J. Chem. 41 (2017) 3667–3676.
[38] Y. Liu, K. Yan, O.K. Okoth, J. Zhang, Biosens. Bioelectron. 74 (2015) 1016–1021.
[39] F. Meng, J. Li, S.K. Cushing, M. Zhi, N. Wu, J. Am. Chem. Soc. 135 (2013) 10286–10289.
[40] W.S. Hummers, R.E. Offeman, J. Am. Chem. Soc. 80 (1958) 1339.
[41] Y. Xu, Z. Lin, X. Zhong, X. Huang, N.O. Weiss, Y. Huang, X. Duan, Nat. Commun. 5 (2014) 4554.
[42] L. Yang, Y. Hu, Q. Wang, Y. Dong, L. Zhang, Anal. Chim. Acta 935 (2016) 104–112.
[43] J.S. Wei, H. Ding, P. Zhang, Y.F. Song, J. Chen, Y.G. Wang, H.M. Xiong, Small 12 (2016) 5927–5934.
[44] N. Hao, R. Hua, S. Chen, Y. Zhang, Z. Zhou, J. Qian, Q. Liu, K. Wang, Biosens. Bioelectron. 101 (2018) 14–20.
[45] D. Carriazo, J. Patino, M.C. Gutierrez, M.L. Ferrer, F. del Monte, RSC Adv. 3 (2013) 13690–13695.
[46] Z. Lu, W. Dai, B. Liu, G. Mo, J. Zhang, J. Ye, J. Ye, J. Colloid Interface Sci. 525 (2018) 86–96.
[47] R. Chen, H.-Y. Wang, J. Miao, H. Yang, B. Liu, Nano Energy 11 (2015) 333–340.
[48] X. Tang, B. Zhang, C. Xiao, H. Zhou, X. Wang, D. He, Sensors Actuators B Chem. 222 (2016) 232–239.
[49] Z. Yu, H. Li, X. Zhang, N. Liu, W. Tan, X. Zhang, L. Zhang, Biosens. Bioelectron. 75 (2016) 161–165.
[50] J. Yang, M. Cho, Y. Lee, Sensors Actuators B Chem. 222 (2016) 674–681.
[51] Y. Ding, Y. Wang, L. Su, M. Bellagamba, H. Zhang, Y. Lei, Biosens. Bioelectron. 26 (2010) 542–548.
[52] H. Heli, J. Pishahang, Electrochim. Acta 123 (2014) 518–526.